RESEARCH ARTICLE

Microstructure changes during failure of PVDF-based photovoltaic backsheets

Stephanie L. Moffitt[1] | Po-Chang Pan[1] | Lakesha Perry[1] | Jared Tracy[3] | Kaushik R. Choudhury[3] | Michael D. Kempe[2] | Xiaohong Gu[1]

[1]Engineering Laboratory, National Institute of Standards and Technology, Gaithersburg, MD, USA

[2]Photovoltaics Research, National Renewable Energy Laboratory, Golden, CO, USA

[3]E. I. du Pont de Nemours and Company, Wilmington, DE, USA

Correspondence
Stephanie L. Moffitt, Engineering Laboratory, National Institute of Standards and Technology, Gaithersburg, MD, USA.
Email: stephanie.moffitt@nist.gov

Funding information
National Institute of Standards and Technology

Abstract

The backsheet layer of a solar module provides a safety and environmental barrier to the high voltages running through the photovoltaic (PV) cells and electrical contacts within the core of the module. However, in the past decade, backsheet cracking has become one of the most observed failure modes in PV module field surveys. In this work, the degradation of polyvinylidene fluoride (PVDF)-based backsheets is explored. Backsheet samples are either exposed to accelerated laboratory aging (UV light, heat, and moisture) or collected from the field. Fourier transform infrared and Raman spectroscopy, fragmentation testing, atomic force and scanning electron microscopy, and small-angle neutron scattering are combined to develop an understanding of how chemistry and microstructure evolve during aging. Chemical degradation, surface pitting, polymer phase changes, and anisotropic polymer domains are all observed in aged backsheet samples. The results provide insight into the degradation mechanisms that lead to cracking and field failure of PVDF-based backsheets. The comparison of aged PVDF-based backsheets helps to lay the groundwork for limiting polymer-based failure modes in PV modules.

KEYWORDS
backsheet degradation, microstructure, polyvinylidene fluoride

1 | INTRODUCTION

Photovoltaic (PV) backsheets are the polymer-based layer on the underside of the PV modules. The backsheet layer provides a safety barrier to the high voltages running through the PV cells and electrical contacts within the core of the module. Backsheets also act as a barrier, protecting the sensitive components within the module core from contaminants. Because of economic pressure to reduce costs, new products and materials are continuously entering the PV backsheet market.[1–4] While some backsheet products have stood the test of time, there are recent reports of wide-spread failure of PV backsheet materials.[5–7] The most common failure modes for backsheets are when layers crack or delaminate and the backsheet can no longer function as an effective barrier.[8,9] Even small, barely visible cracks can quickly progress to dramatic failure modes, including total backsheet cracking and electrical arcing.[6] Therefore, rigorous testing through accelerated aging and materials characterization is important. While accelerated aging standards for testing PV modules exist, there is significant doubt that these standards will effectively screen new backsheet materials for long-term performance.[10] Newer accelerated aging protocols, which focus on combined stresses, have been able to replicate field failures in a number of PV backsheet materials.[10,11] However, an understanding of backsheet materials degradation pathways is needed to ensure that newly introduced materials will meet module target service lifetimes.
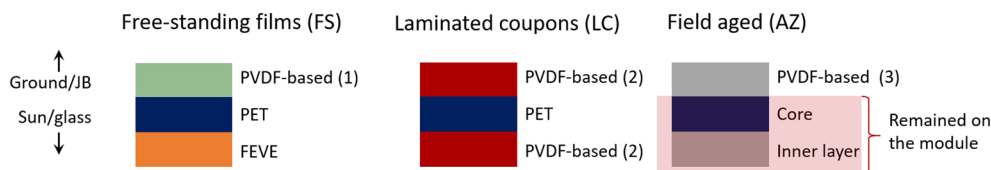
FIGURE 1 Schematic of the backsheet architectures for the three different sample types. The source of the PVDF-based outer layers is not confirmed and may be different; further details are in the Discussion section. Directions of the ground/junction box (JB) and sun/glass are indicated with arrows. Schematic is not to scale and does not depict adhesive layers. [Colour figure can be viewed at wileyonlinelibrary.com]
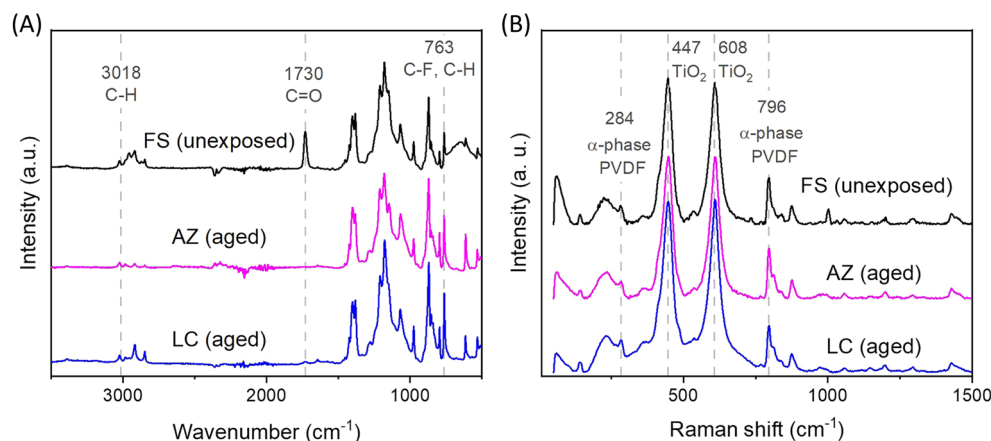

FIGURE 2 (A) Representative FTIR-ATR spectra from the outer, air-side layer of each type of sample: free-standing film (FS [unexposed], top, black), field aged in Arizona (AZ, middle, pink), and laminated coupon (LC, bottom, blue). (B) Representative Raman spectra from outer, air-side layer of the FS (top, black), AZ (middle, pink), and LC (bottom, blue) samples [Colour figure can be viewed at wileyonlinelibrary.com]

Polyvinylidene fluoride (PVDF) polymers have been used as a material in laminate PV backsheets since 2003.[12] Laminated PV backsheets, like the ones explored here (Figure 1), consist of a fluoropolymer outer layer, which provides weathering protection, and a polyethylene terephthalate (PET) core, which provides mechanical strength and electrical insulation. PVDF-based backsheets were anticipated to perform well in the field because fluoropolymers generally have excellent ultraviolet light (UV) durability; PVDF materials in particular have been shown to be excellent exterior architecture coatings.[13,14] In addition, PVDF-based backsheets performed well under current standards-based testing. However, recent field and accelerated aging studies have begun to document the failure of some PVDF-based backsheets.[5,15]

In this work, we investigate the degradation modes in aged PVDF-based backsheets. Three different aging protocols are explored: accelerated laboratory aging of free-standing films under IEC62887 A3 (UV light, heat, and humidity), accelerated laboratory aging of coupons using the Solder-Bump test,[16] and field-aging of a full-scale module in Arizona, USA. Sample chemistry was characterized with attenuated total reflection Fourier transform infrared (ATR-FTIR) and Raman spectroscopies. A loss of polymethyl methacrylate (PMMA) content on the outer surface was observed during aging in samples that contained a PVDF/PMMA blend. The influence of aging on the surface microstructure is investigated through both atomic force and scanning electron microscopies (AFM and SEM). Previous work has shown that differences in PVDF polymer microstructure can be tied to differences in polymer durability.[17] Surface pitting, microcracks, and indicators of polymer crystalline phase change were all observed in aged backsheet samples. Sample-averaged crystalline domain structures were studied through small-angle neutron scattering (SANS). An anisotropy within the crystalline domain ordering between the machine and transverse

direction of the polymer was observed; the structural anisotropy mirrored the measured mechanical anisotropy in the elongation at break observed with tensile testing. The comparison of the chemistry and microstructure of aged samples provides new insights for understanding and replicating the degradation mechanisms that lead to cracking and field failure of PVDF-based backsheets.

2 | METHODS

2.1 | Samples

All samples were commercially sourced PVDF-based backsheets. These backsheets are made of three primary layers (Figure 1). The outer-most layer is PVDF-based (Figure 2). The core layer is made of PET. The inner-most layer binds to the encapsulant and is made of either another PVDF-based layer or fluoroethylene vinyl ether (FEVE). Titania (TiO_2) pigments in the PVDF-based outer layers give all samples a white appearance (Figure 1). The source of the PVDF-based layer is not known for each case and is not assumed to be from the same manufacturer.

Samples were aged in one of three ways: accelerated aging of free-standing films (FS), accelerated aging of a laminated coupon (LC), or field aged as part of a module deployed in Arizona for 7 years (AZ) (Figure 1).

The FS samples were aged under A3 weathering condition in accordance with IEC 62788-7-2: 0.8 W/m²/nm irradiation at 340 nm, 20% relative humidity (RH), and chamber air temperature at 65 °C. FS samples were aged up to 4000 h.[18] With respect to UV-dose, 4000 h at 0.8 W/m²/nm irradiation provides a dose comparable with 20 years

outdoors in Arizona with 12% ground albedo. Accelerated aging of LC coupons employed the Solder-Bump test.[16] PVDF-based backsheets were laminated to glass coupons 50.8 mm by 76.2 mm in size. During lamination, a length of solder was either pressed into the backsheet to create a trench or was incorporated into the ethylene-vinyl acetate (EVA) encapsulant layer to create a ridge (supplemental information [SI], Figure S1). After lamination, the coupons were exposed (on either the glass/front-side or the backsheet/back side) to 500 h of the A3 weather condition (as described above), followed by 100 thermal cycles (TC) where the temperature was cycled between $-40\,°C$ and $85\,°C$ with a dwell of 10 min at each temperature maxima and a ramp rate of $100\,°C/h$.[19] The thermal cycles were performed in the dark with uncontrolled, ambient humidity. The A3 and TC exposure cycle was then repeated four more times for a total exposure of 2500 h A3 and 500 TCs. Further details on the Solder Bump test can be found in our previous work.[16] The AZ sample was removed from a 7-year-old field-aged module in Arizona. The module was part of a PV-field where backsheet cracking and delamination were occurring. It was reported that backsheet cracks were often observed in regions near busbars and were often oriented along the machine direction of the polymer backsheet.

2.2 | Spectroscopy

FTIR was performed in ATR mode using a Nicolet 6700 spectrometer with a diamond crystal (about 2 μm penetration depth). A total of 64 scans were made between $650\ cm^{-1}$ and $4000\ cm^{-1}$ with a resolution of $4\ cm^{-1}$. For the FS samples, the progressive decrease in the carbonyl peak was quantified by calculating the ratio of the peak intensity at $1730\ cm^{-1}$ (attributable to C=O stretching) versus the peak intensity at $830\ cm^{-1}$ (attributable to CH_2 rocking on PVDF).[20] Raman spectroscopy was performed on a Senterra II Confocal Raman Microscope (Bruker, Germany) with excitation wavelength of 785 nm (about 12 μm penetration depth),[21] 10 mW laser power, and $4\ cm^{-1}$ spectral resolution in the range of $50\ cm^{-1}$ to $3640\ cm^{-1}$.

2.3 | Microscopy

Scanning electron microscopy (SEM) images were taken with a JEOL JSM-7600F microscope. Samples were sputtered with a layer of amorphous carbon, before imaging to limit charging effects. Surface microstructures were characterized using a Bruker Dimension Icon atomic force microscopy (AFM) in tapping mode. Both height and phase images were recorded with a (512 × 512) pixel resolution at a scan rate of 0.5 Hz by an antimony doped silicon probe with a spring constant of 40 N/m under ambient conditions (24 °C, ≈ 45% RH).

2.4 | Fragmentation testing

Rectangular strips (40 mm × 5 mm) of aged PVDF-based backsheets were pulled in uniaxial tension along their transverse direction on a

miniaturized tensile test device (MTI Instruments, USA) mounted under the laser scanning confocal microscope. The miniaturized tensile tester has a max load capacity of 450 N (corresponding to a 100 lb. weight) with a load accuracy of ± 0.9 N and position accuracy of ±20 nm. During tension, a step strain was applied with an increment of 1% every 5 min with a strain rate of $1.4 \times 10^{-4}\ s^{-1}$ at a gauge length of 35 mm, and the load–displacement history was recorded automatically. During each 5-min step, strain was applied for 71.4 s, and the remaining time was used to image the sample with a confocal microscope (SI, Figure S4).

2.5 | Neutron scattering

Small-angle neutron scattering (SANS) was performed on the NG-7 SANS instrument at the NIST Center for Neutron Research.[22] Samples were measured in transmission geometry at a sample-to-detector distance of 4 m. Because neutrons penetrate the full thickness of the backsheet, the outer-most PVDF-based layers were removed and measured to avoid additional scattering from the PET, EVA, and FEVE layers. PVDF-based layers were removed from the backsheets stack by soaking the samples in acetone for 24 h to weaken the adhesive holding the layers together. Previous work has shown that this acetone procedure does not alter the mechanical properties nor the crystal structure of the PVDF-based layers.[23,24]

3 | RESULTS AND DISCUSSION

3.1 | Chemistry of samples

FTIR spectra confirm that the outer-most layer in each type of sample is PVDF-based. As seen in Figure 2, a sharp peak at $763\ cm^{-1}$ in each spectrum is attributed to a combination of C-H and C-F bonds.[25,26] An additional peak at $1730\ cm^{-1}$, which is characteristic of C=O stretching, is also visible in the FS spectra, which indicates that the FS outer layer is not pure PVDF. Likely, the FS backsheet samples are PVDF/PMMA blends, with ranging levels of PMMA in the outer, PVDF-based layer.[27] PMMA, an acrylic modifier, is blended with PVDF to lower costs, improve adhesion, and facilitate the incorporation of pigments.[14,27–29] Acrylic modifiers can also be added to PVDF to increase hardness and improve gloss.[14] However, multiple material properties including UV durability, drawability, and elongation at break can be influenced by the PVDF/PMMA ratio.[28,30,31]

The LC samples are understood to have a thin, unpigmented outer layer of essentially pure PVDF. As such, the LC samples lack a strong peak at $1730\ cm^{-1}$ in the FTIR spectra. A similar absence of a peak at $1730\ cm^{-1}$ is seen for the AZ sample and suggests that this sample has a similar architecture. While it is possible that all speculative PMMA content in the LC and AZ sample could be substantially degraded and thus no longer detected as carbonyl peaks, this scenario is unlikely. Figure 5B illustrates how the PMMA peak at $1730\ cm^{-1}$

decreases as a function of aging time for the FS samples but does not reach undetectable levels.

Raman spectra of the FS, LC, and AZ samples (Figure 2B) are similar. Peaks at 447 and 608 cm^{-1} indicate that rutile TiO_2 is present in all samples.[32] The presence of these peaks is anticipated, as incorporation of TiO_2 as pigment particles is common in white backsheets. It is important to note that the penetration depth of Raman spectroscopy is deeper than FTIR-ATR.[21] Thus, while the FTIR spectra (Figure 2A) suggests that the outermost layer of the LC and AZ samples is pure PVDF, the TiO_2 pigments seen in the Raman spectra (Figure 2B) likely lie below the pure PVDF layer in a second PVDF/PMMA blended layer.

3.2 | Free-standing film samples (FS)

Free-standing PVDF-based backsheets were aged under the A3 condition, as described above. Though the outer-most PVDF based layer (Figure 1) was the focus of our work, the free-standing nature of the films enabled micro-FTIR cross-sectional measurements (SI, Figure S2). These measurements revealed that the PVDF-based outer layer is bonded with a polyester-based adhesive to a PET core. The PET core provides mechanical strength and acts as a dielectric. The inner-most, cell-side layer of the FS backsheets was a thin FEVE coating.

AFM topography of the fresh, unaged FS sample reveals submicron roughness (Figure 3A). The surface texturing appears to be dominated by spherical-like protruding structures several hundred nanometers in diameter. These structures are probably due to titania pigments distributed in the polymeric matrix (Figure 2B). After exposure to A3 aging conditions, the spherical structures become less prevalent and are replaced by pits of a comparable size (Figure 3B). The submicron pit structures are more clearly imaged by SEM (Figure 4A).

The spherical-like structures observed on the surface through AFM (Figure 3A) and SEM (Figure 4) are of comparable size to typical titania pigment particles.[33,34] The particles also appear much brighter in the SEM images, as is expected for heavier elements.[35] As mentioned above, Raman spectroscopy has confirmed that titania is present on the surface of the FS samples (Figure 2B). Thus, we propose that the surface pitting of the aged FS samples is due to a loss of titania pigment particles. It is reasonable to suggest that if the titania particles were released, a pit of similar size would be left behind.

The surface pitting may be further facilitated by a loss of PMMA content due to the photocatalytic effect of the titania particles. In the FS sample, an increase in accelerated aging exposure time results in a decrease in the carbonyl peak at 1730 cm^{-1} (Figure 5). Quantification of the decline in peak intensity is shown in Figure 5B. The decline in the carbonyl peak is persistent. In contrast, the C-F peak at 1180 cm^{-1} remains largely unchanged throughout the full exposure. As stated above, the carbonyl peak likely comes from PMMA content blended into the PVDF polymer.[27] Thus, the FTIR results suggest that the PMMA content of the outer layer undergoes significant chemical degradation while the PVDF content remains stable.[27,36] Given that in
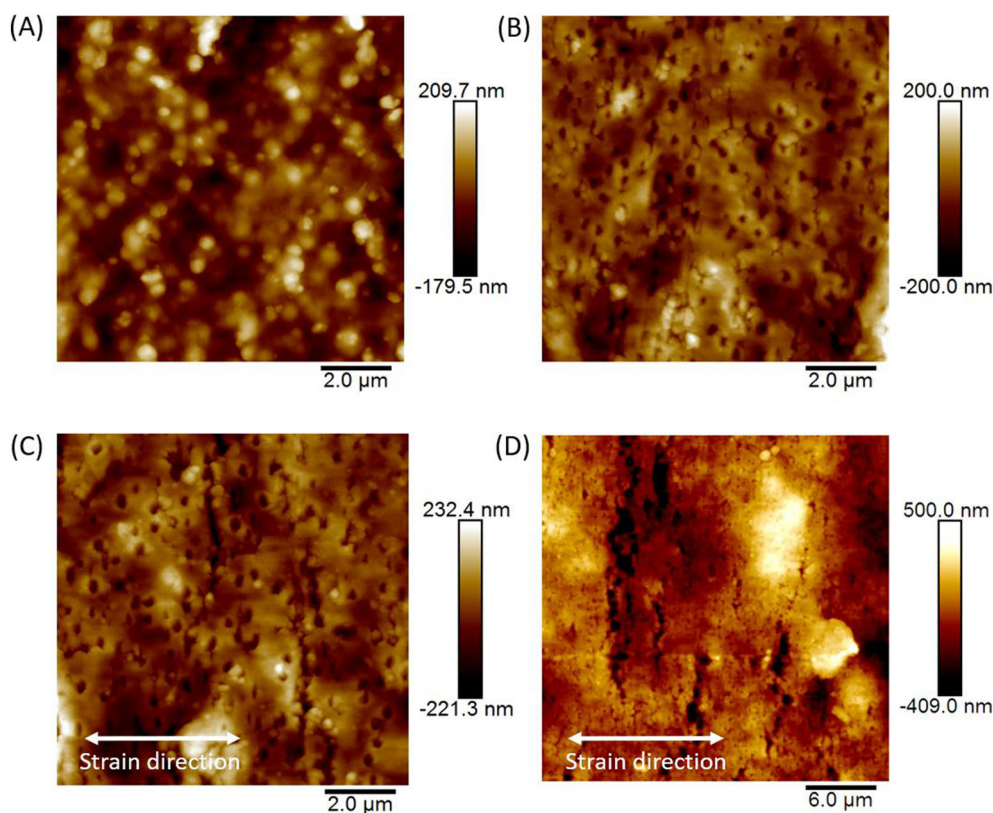

FIGURE 3 AFM topography of FS sample: (A) unaged, (B) after 4000 h of aging, (C) after 4000 h of aging and application of 5% tensile strain in the transverse direction (TD, direction shown with white arrow), and (D) after 4000 h of aging and application of 25% TD tensile strain (direction shown with white arrow) [Colour figure can be viewed at wileyonlinelibrary.com]

FIGURE 4 SEM images of FS samples exposed to (A) 4000 h A3 aging and (B–D) 4000 h of aging and application of 5% tensile strain applied in the TD direction [Colour figure can be viewed at wileyonlinelibrary.com]
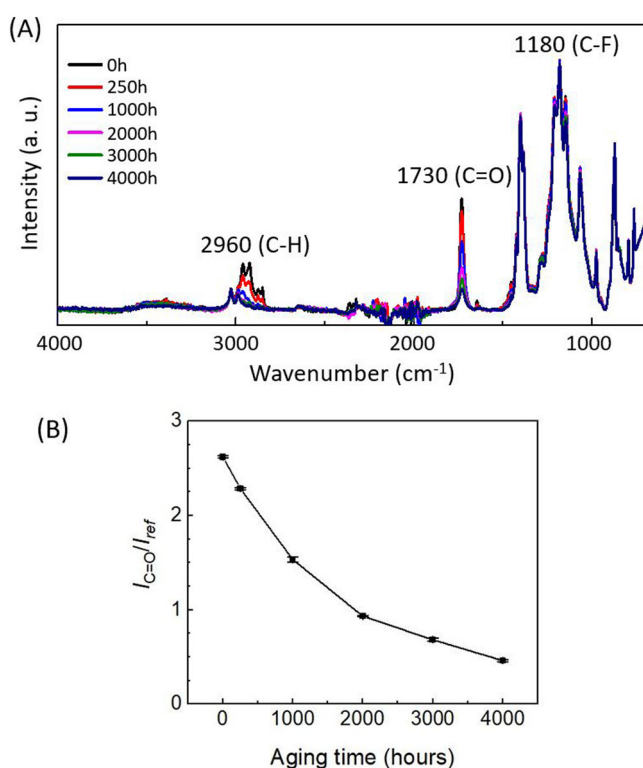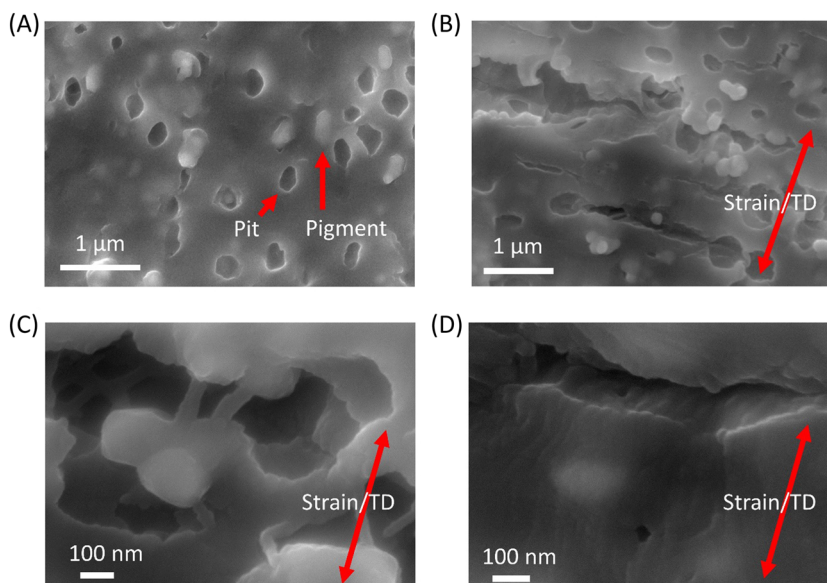

FIGURE 5 (A) Progression of representative FTIR-ATR spectra of the FS samples as a function of exposure time. (B) Quantification of the reduction in the intensity (peak height after background subtraction) of the carbonyl peak versus the intensity of the reference peak (830 cm^{-1}, PVDF CH$_2$ rocking), which reveals the progressive loss in PMMA content as a function of aging. Error bars represent the standard deviation from multiple measurement spots taken at each aging time point and are smaller than the data points. [Colour figure can be viewed at wileyonlinelibrary.com]

PMMA/PVDF blends, PMMA remains in the amorphous region of the polymer and pigment particles are more likely to be embedded within the amorphous region of the polymer matrix, it is reasonable to suggest that PMMA chemical degradation facilitates the loss of titania pigment particles.[36] Furthermore, it is possible that the photocatalytic effect of titania may accelerate the loss in PMMA content around the pigment particles.

Despite the presence of surface pits that could serve as a nucleation site for fracture, no significant structural degradation (i.e., cracking) is observed after A3 aging of the FS samples before strain is applied. We note that the free-standing nature of the samples during aging removes strain effects from thermal mismatch between the backsheet and other modules components (e.g., glass and busbars). Thus, strain was applied post-aging employing the fragmentation test described above. Once tensile strain is applied, surface cracks form in the aged samples (Figures 3C,D and 4B–D). Microcracks observed with AFM are on the order of microns and confocal images of these strained samples (SI, Figure S4) do not show microcracks. The microcracks appear to form as a coalescence of surface pits (Figure 4B). The cracks form perpendicular to the strain direction. Fibrous structures bridge the cracks (Figure 4C).

3.3 | Laminated coupon sample (LC)

Like the FS samples, the LC sample was aged using the A3 condition (described above), but with a thermal cycling step added at the end. Unlike the FS sample, the outermost layer of the LC sample is pure PVDF and contains no PMMA or titania pigments (as discussed in the *Chemistry of Samples* section). Without PMMA or surface pigments at the top surface layer, no surface pits form during aging, as seen in

AFM images of the aged LC surface (Figure 6). Similarly, the AZ sample, which also has a pure-PVDF surface layer, also does not show signs of surface pitting (Figure 7).

An additional and important difference between the FS and LC samples is the lamination of the backsheet to a glass coupon with pieces of solder wire before aging. The inclusion of solder wire results in a visible ridge or trench when the wire is laminated either between the glass and polymer layers (and remains) or outside the module (and is subsequently removed), respectively (SI, Figure S1). These defects

created locations in the coupons where the backsheet outer and inner layers were either in tension and compression (ridge) or compression and tension (trench). Thus, when UV light was exposed directly to the backsheet and a thermal cycling step was applied, visible cracks formed at the localized stresses in the ridge and trench regions of the coupons (SI, Figure S1).[16]

AFM images demonstrate changes in the surface morphology near the cracked regions. Away from the crack (Figure 6B,C) the surface microstructure of the LC samples is made of spherulite
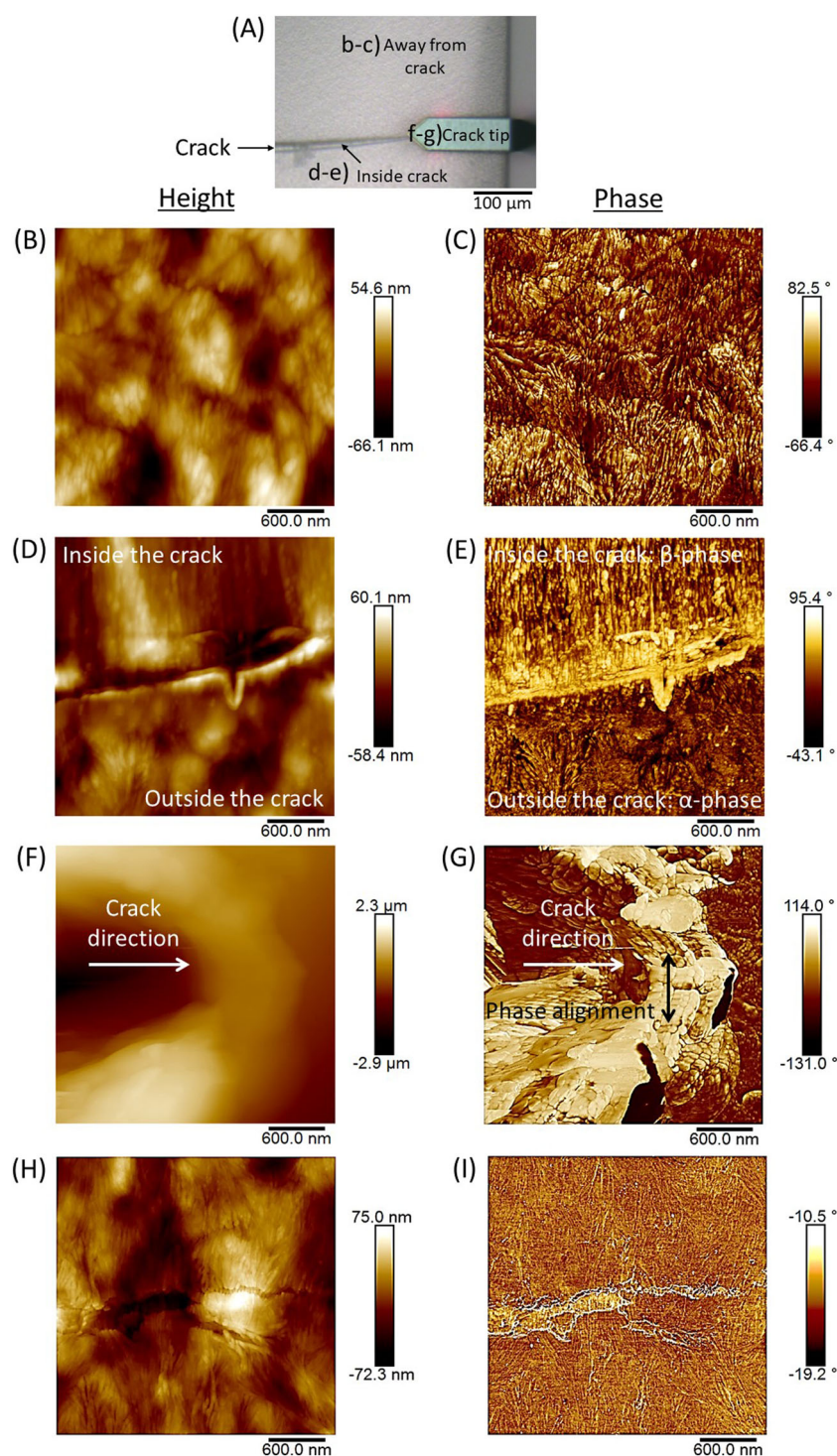

FIGURE 6 (A) Optical image of representative crack in LC sample with representative AFM collection points indicated. AFM height (left) and phase (right) images taken of the LC samples surface collected (B, C) away from the crack, (D, E) on the edge and inside the crack, (F, G) at the crack tip, and (H, I) at a micro-crack. In F and G, a white arrow shows the crack direction and black arrows in highlights the direction of the observed morphology alignment. [Colour figure can be viewed at wileyonlinelibrary.com]

FIGURE 7 (A) High magnification AFM phase image of AZ sample before the application of 5% strain and (B) AFM topographic image of AZ sample after the application of 5% strain in the TD as indicated [Colour figure can be viewed at wileyonlinelibrary.com]
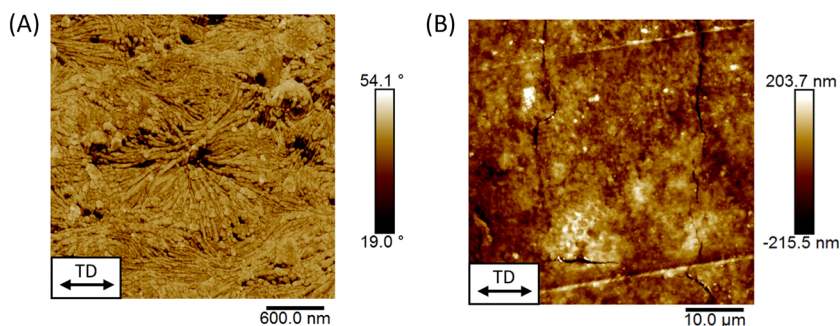
structures, the hallmark of α phase PVDF.[35,37] Inside the crack, AFM reveals a significant change in the microstructure. Instead of spherulite bundles, the structure becomes more ordered and directional. Furthermore, using the intermittent contact mode on the AFM and monitoring the phase signal, a significant phase contrast between the region inside versus outside the crack was observed (Figure 6E), indicating differences in mechanical properties (e.g., stiffness, adhesion, dissipation, etc.) between these regions. These results suggest that the PVDF polymer within the crack has undergone a phase transition from α to β phase due to significant deformation during cracking. The β phase of PVDF is the elongated, all-trans polar conformation of PVDF, while the α phase is the gauche, nonpolar conformation which creates a helix-type structure.[38] The polymer morphology at the crack tip (Figure 6G) is ordered and directional, as is consistent with β phase PVDF.[37] Previous work has shown that α to β phase transitions can occur in cracked and strained pure PVDF polymers.[39] Further, α to β phase transformation has been observed to be part of the crack propagation mechanisms in pure PVDF.[40] Figure 6H shows that cracks can also occur in the rigid lamella of the spherulites, breaking the lamella instead of causing phase transformation of crystallites. Additional work is planned to conduct an in-depth X-ray scattering study to investigate α to β phase transitions during crack growth in aged PVDF backsheets. However, the study is outside the scope of the current manuscript.

3.4 | Arizona field-aged sample (AZ)

The AZ sample was part of a full-scale PV module that was pulled from the field when backsheet cracking and delamination were observed. It was reported that backsheet cracks were observed in regions near busbars and often were oriented along the machine direction of the polymer backsheet. The sample in this work is a piece of the outer-most layer of the backsheet, the PVDF-based layer, which had begun to delaminate. It came from an area between two busbar ribbons where no cracks were observed. As seen in Figure 7A, the unstrained AZ sample surface morphology is dominated by spherulite structures, indicative of PVDF α phase. This morphology mirrors the surface region away from the cracks in the LC samples (Figure 6B, C). As stated above, both the LC sample and the AZ sample surfaces were free of the pits observed in the aged FS samples. Though not explicitly confirmed, we believe the outer PVDF-based layer of these
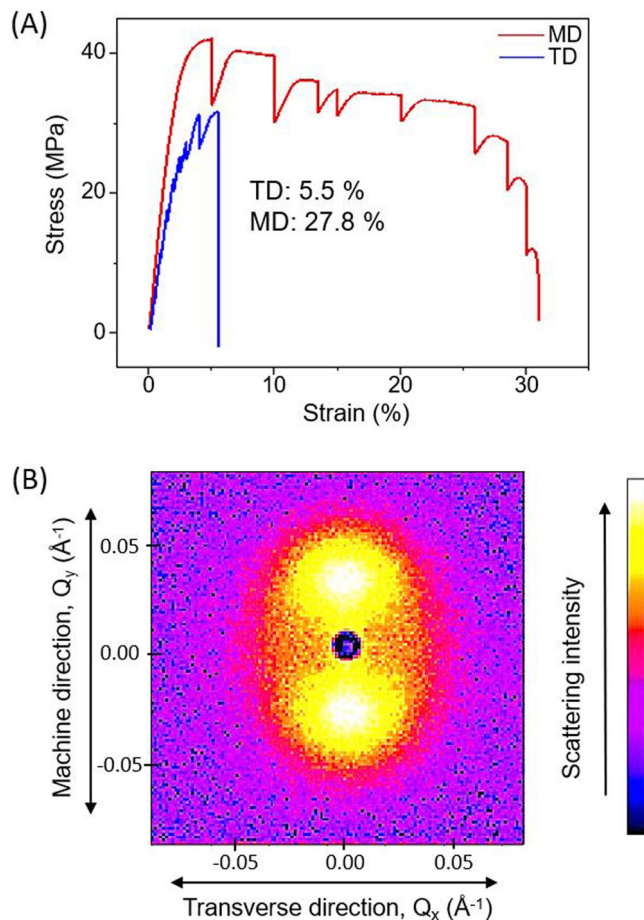

FIGURE 8 (A) Typical stress–strain curve for the AZ sample when tensile strain was applied in either the machine or transverse direction (MD or TD). The elongation at break is recorded in the inset for both the TD and MD. (B) 4-m SANS pattern of the AZ sample [Colour figure can be viewed at wileyonlinelibrary.com]

backsheets is from the same manufacturer and contains a thin layer of pure-PVDF (Figure 1). Thus, the lack of surface pitting in the aged LC and AZ samples is likely due to the lack of PMMA and pigment content at the surface. With no PMMA to degrade at the surface and facilitate the loss of pigments, the pitting mechanism does not occur.

To test the crack propensity of this fielded backsheet, small strains were applied to sections of the AZ sample in both the machine direction (MD) and the transverse direction (TD) using the

TABLE 1 Summary of results for three PVDF-based backsheet samples

	Free standing (FS)	Laminated coupon (LC)	Field aged (AZ)
Chemistry	**Blend** of PVDF, PMMA, and rutile TiO_2 pigments During aging exposure, **loss of PMMA**	**Thin** outer layer of **pure PVDF** Below pure PVDF layer, second layer contains rutile TiO_2 pigments	**Thin** outer layer of **pure PVDF** Below pure PVDF layer, second layer contains rutile TiO_2 pigments
Morphology (after aging)	After aging, surface pigments are lost, leaving **surface pits** No cracks observed	Aged surface does not show pitting Macro **cracks near busbar** α phase spherulites away from cracks. **α to β phase** transition at crack tips	Aged surface does not show pitting Macro **cracks near busbars** on full module (not retrieved) α phase spherulites away from cracks
Morphology (w/fragmentation test)	**Pits coalesce** to form surface cracks Global increase in morphology alignment (likely β phase)		Cracks form more easily when strained in transvers direction, correlates with **anisotropy of crystallites** Global increase in morphology alignment (likely β phase)

fragmentation test described above. Unlike the LC sample, a prominent change in the surface was not observed near cracks induced by the fragmentation test. Rather, the morphology changes were not limited to the cracks and instead occurred more globally throughout the sample (SI, Figure S5c). This difference is likely because during the fragmentation test, strain is applied globally across the whole film, rather than locally by inhomogeneities induced by a busbar (as in the LC sample or in the regions of the AZ module backsheet that were not retrieved). The observation of a more subtle and more global change in surface morphology is also seen in the FS samples (SI, Figure S5b). Thus, while the small strains (≤5%) applied by the fragmentation test successfully reproduce field cracking on a macro-level, the microstructure changes of the FS and AZ samples are smaller and more global than those seen in the LC sample. This difference is attributed to the different nature of the strain application.

During fragmentation testing specific strain is added gradually in steps to observe the fracture behavior. This step-based approach produces stepped stress–strain curves (Figure 8A). The elongation at break was significantly weaker in the TD (5.5%) compared to the MD (27.8 %) (Figure 8A). This result is in-line with the field observation that crack formation was often oriented along the machine direction. An AFM topographic image of the AZ sample after stretching 5% in the TD is shown in Figure 7B. Cracks appeared perpendicular to the TD (aligned with the MD). Though the AZ sample was not cracked initially, the fragmentation test revealed that the material was predisposed to crack once a small strain was applied. This may explain why the fielded module was cracking near the module busbars; regions along busbars are anticipated to be exposed to strain effects due variations in module topology.

To investigate whether the significant anisotropy in the tensile strength was related to anisotropy in the polymer structure, small-angle neutron scattering was performed on the AZ and FS samples to characterize the sample-averaged microstructure. Pronounced anisotropic scattering is seen near 0.04 Å^{-1}, with higher intensity in the machine direction of the polymer. Scattering in this range is anticipated to originate from the long-period spacing (i.e., the spacing between crystalline domains) of the PVDF polymer.[41] It is likely that the processing of the polymer induced preferred orientation of the crystalline domains. The anisotropy in the microstructure may explain the anisotropy in the tensile strength. Earlier studies have seen similar anisotropy in the tensile modulus of PVDF/PMMA/TiO_2. In the work by Hosoda and Yamada, the TD had a lower tensile modulus than the MD.[35] The authors attributed this behavior to the anisotropy in the crystalline structure of the polymer where the crystals are oriented in the MD. When strained in the MD, the amorphous regions between the lamella enable the spherulites to deform, whereas in the TD more strain is placed on the rigid lamella which break instead of deforming. This results in less than 20% elongation at break for the TD versus over 200% for the MD.[35]

4 | CONCLUSION

PVDF-based backsheet samples were exposed to three different aging conditions. Lab-aged samples were exposed to UV light, heat, and humidity as either free-standing films or laminated coupons. In addition, a sample was collected from a module deployed in Arizona, USA, for 7 years; we believe the field-aged modules used the same PVDF-based backsheet as the laminated coupon samples. The aging of these materials was studied, including the influence of aging on the surface microstructure. A summary of the results from this investigation is presented in Table 1. Materials characterization included fragmentation testing, SANS, SEM, AFM, Raman, and ATR-FTIR spectroscopies. Free standing films were observed to develop submicron sized surface pits after aging. Surface pitting was associated with chemical degradation within the PMMA component of the PVDF/PMMA backsheet outer layer due to the photocatalytic effect of titania and the loss of submicron sized titania pigment particles. With the application of strain, the surface pits coalesced to form larger surface cracks. Laminated coupons cracked during

accelerated aging; large cracks were visible along the ridge and trench regions where local residual strain was induced by the solder wire. AFM images revealed differences in microstructure between the areas inside verses outside the cracks. This difference in surface morphology suggests that α to β phase transition may occur near cracked regions under significant deformation in PVDF-based backsheets and may be involved in the crack propagation mechanism. In the field-aged sample from Arizona, a notable anisotropy in tensile strengths was measured. This anisotropy was mirrored in the anisotropy of the crystalline domains, as observed by SANS. From the range of aged PVDF-based backsheet samples studied in this work, it is evident that several different materials characteristics (i.e., polymer composition, photocatalytic pigments, and anisotropic mechanical properties) and especially microstructural changes (i.e., surface pitting, phase changes, and anisotropic phase ordering) can play a role in backsheet failure. The insights provided in this work lay the foundation for future studies to delve deeper into the degradation mechanisms of PVDF-based backsheets.

DISCLAIMER STATEMENT

Trade names and commercial products are identified in this proceeding to specify the experimental procedures in adequate detail. This identification does not imply recommendation or endorsement by the authors or by the National Institute of Standards and Technology, nor does it imply that the products identified are necessarily the best available for the purpose.

DATA AVAILABILITY STATEMENT
The data that support the findings of this study are available from the corresponding author upon reasonable request.

ORCID
Stephanie L. Moffitt 🅳 https://orcid.org/0000-0002-5934-9771
Xiaohong Gu 🅳 https://orcid.org/0000-0002-8812-9540

REFERENCES
1. Hutchins M. "Transparent backsheet: well it's swan for the money …," PV Magazine, p. 1, 2019.
2. Bellini E. "New solar module backsheet based on polyamide," PV Magazine, pp. 1-9, 2020.
3. Bazilian M, Onyeji I, Liebreich M, et al. Re-considering the economics of photovoltaic power. *Renew Energy*. 2013;53:329-338. doi:10.1016/j.renene.2012.11.029
4. Fairbrother A, Boyd M, Lyu Y, et al. Differential degradation patterns of photovoltaic backsheets at the array. *Sol Energy*. 2018;163:62-69. doi:10.1016/j.solener.2018.01.072
5. Tracy J, Gambogi W, Felder T, et al. "Survey of material degradation in globally fielded PV modules," in IEEE Photovoltaic Specialists Conference. 2019;874-879.
6. Felder T, Hu H, Gambogi W, Choudhury KR, Garreau-lles L, Trout TJ. "Field study and analysis of backsheet degradation in 450MW + PV installations," in 4th Atlas-NIST Workshop on Photovoltaic Materials Durability. 2017;1-16.
7. Groenendaal B, Gifford J. Reports of backsheet failures at 75 MW Mulilo Sonnedix Prieska solar farm in South Africa. *PV Magazine*. 2020;1-8.
8. Wohlgemuth JH. "Assessing the trends in module field failures," in IEEE 7th World Conference on Photovoltaic Energy Conversion. 2018;92-97.
9. Aghaei M, Fairbrother A, Gok A, et al. Review of degradation and failure phenomena in photovoltaic modules. *Renew Sustain Energy Rev*. 2022;159:112160.
10. Owen-Bellini M, Hacke P, Miller DC, et al. Advancing reliability assessments of photovoltaic modules and materials using combined-accelerated stress testing. *Prog Photovoltaics Res Appl*. 2021;29(1):64-82. doi:10.1002/pip.3342
11. Gambogi W, Yu BL, Felder T, et al. "Development of accelerated test sequences to assess long term durability of PV modules," in IEEE Photovoltaic Specialists Conference. 2019;2406-2410.
12. DeBergalis M. Fluoropolymer films in the photovoltaic industry. *J Fluourine Chem*. 2004;125(8):1255-1257. doi:10.1016/j.jfluchem.2004.05.013
13. Wood KA, Cypcar C, Hedhli L. Predicting the exterior durability of new fluoropolymer coatings. *J Fluor Chem*. 2000;104(1):63-71. doi:10.1016/S0022-1139(00)00228-1
14. Iezzi RA. "Polyvinylidene fluoride-based coatings technology," in ASM Handbook, vol. 5B, no. Protective Organic Coatings. 2015;80-87.
15. Owen-Bellini M, Hacke P, Spataru SV, Miller DC, Kempe M. "Combined-accelerated stress testing for advanced reliability assessment of photovoltaic modules," in 35th European Photovoltaic Solar Energy Conference and Exhibition. 2018;1101-1105.
16. Kempe MD, Lockman T, Morse J. "Development of testing methods to predict cracking in photovoltaic backsheets," in IEEE Photovoltaic Specialists Conference, 2019;2411-2416.
17. Sung LP, Vicini S, Ho DL, Hedhli L, Olmstead C, Wood KA. Effect of microstructure of fluorinated acrylic coatings on UV degradation testing. *Polymer*. 2004;45(19):6639-6646.
18. Gambogi WJ, Yu B-L, Trout TJ, Phillips N, MacMaster SW, Felder TC. "Comparison of higher irradiance and black panel temperature UV backsheet exposures to field performance," in Proceedings of SPIE. 2017, vol. 1037002, no. August 2017, p. 3.
19. International Electrotechnical Commission. IEC 61215-2: terrestrial photovoltaic (PV) modules—design qualification and type approval—part 2: test procedures. 2016;28-29.
20. Kobayashi M, Tashiro K, Tadokoro H. Molecular vibrations of three crystal forms of poly (vinylidene fluoride). *Macromolecules*. 1975;8(2):158-171. doi:10.1021/ma60044a013
21. Adar F. Depth resolution of the Raman microscope: optical limitations and sample characteristics. *Spectroscopy*. 2010;0(0):1-6.
22. "www.nist.gov/ncnr/ng7-sans-small-angle-neutron-scattering".
23. Yuen PY, Moffitt SL, Novoa FD, Schelhas LS, Dauskardt RH. Tearing and reliability of photvoltaic module backsheets. *Prog Photovoltaics Res Appl*. 2019;27(8):693-705. doi:10.1002/pip.3144
24. Moffitt SL, Yuen PY, Owen-Bellini M, et al. "Understanding PV polymer backsheet degradation through X-ray scattering," in IEEE Photovoltaic Specialists Conference. 2019;2394-2397.
25. Lanceros-Méndez S, Mano JF, Costa AM, Schmidt VH. FTIR and DSC studies of mechanically deformed β-PVDF films. *J Macromol Sci – Phys B*. 2001;40(3–4):517-527. doi:10.1081/MB-100106174
26. Betz N, Le Moël A, Balanzat E, et al. A FTIR study of PVDF irradiated by means of swift heavy ions. *J Polym Sci B*. 1994;32(8):1493-1502. doi:10.1002/polb.1994.090320821
27. Huang C, Zhang L. Miscibility of poly (vinylidene fluoride) and atactic poly (methyl methacrylate). *J Appl Polym Sci*. 2004;92(1):1-5. doi:10.1002/app.13564
28. Sung LP, Gu X, Ho DL, Landis FA, Nguyen D. Effect of composition and processing condition on microstructural properties and durability

of fluoropolymer/acrylic blends. *Chinese J Polym Sci*. 2009;27(1): 59-69. doi:10.1142/S0256767909003650

29. Bussi P. "Kynar(R) films novel PVDF multilayer blown films," in MBS Specialty Plastic Films, 2001, vol. October 24.

30. Tanaka A, Kojima Y. Application of poly (vinylidene fluoride) and poly (methyl methacrylate) blends to optical discs. *Kobunshi Ronbunshu*. 1990;47(12):989-991. doi:10.1295/koron.47.989

31. Cebe P, Chung SY. Tensile behaviour of blends of poly (vinylidene fluoride) with poly (methyl methacrylate). *J Mater Sci*. 1990;25(5): 2367-2378. doi:10.1007/BF00638030

32. Swamy V. Size-dependent modifications of the first-order Raman spectra of nanostructured rutile TiO_2. *Phys Rev B - Condens Matter Mater Phys*. 2008;77(19):15-18.

33. Hata K, Kimoto R, Sone K. "Backsheet chalking—theoretical background and relation to backsheet cracking and insulation failures," in 35th European Photovoltaic Solar Energy Conference and Exhibition. 2018;9(2):3-7.

34. Watson S, Tseng IH, Marray T, Pellegrin B, Comte J. Pigment and nanofiller photoreactivity database. *J Coatings Technol Res*. 2012;9(4): 443-451. doi:10.1007/s11998-012-9408-8

35. Hosoda T, Yamada T. Effect of TiO_2 on morphology and mechanical properties of PVDF/PMMA blend films prepared by melt casting process. *J Appl Polym Sci*. 2014;131(13):40454. doi:10.1002/app. 40454

36. Sharma M, Madras G, Bose S. Unique nanoporous antibacterial membranes derived through crystallization induced phase separation in PVDF/PMMA blends. *J Mater Chem A*. 2015;3(11):5991-6003. doi:10.1039/C5TA00237K

37. Sencadas V, Gregorio R, Lanceros-Méndez S. α to β phase transformation and microestructural changes of PVDF films induced by uniaxial stretch. *J Macromol Sci Part B Phys*. 2009;48(3):514-525. doi:10.1080/00222340902837527

38. Ameduri B. From vinylidene fluoride (VDF) to the applications of VDF-containing polymers and copolymers: recent developments and future trends. *Chem Rev*. 2009;108(12):6632-6686.

39. Li L, Zhang M, Rong M, Ruan W. Studies on the transformation process of PVDF from α to β phase by stretching. *RSC Adv*. 2014;4(8): 3938-3943. doi:10.1039/C3RA45134H

40. Maier GA, Wallner G, Lang RW, Fratzl P. Structural changes during plastic deformation at crack tips in PVDF films: a scanning X-ray scattering study. *Macromolecules*. 2005;38(14):6099-6105. doi:10.1021/ ma050390f

41. Cakmak M, Teitge A, Zachmann HG, White JL. On-line small-angle and wide-angle x-ray scattering studies on melt-spinning poly (vinylidene fluoride) tape using synchrotron radiation. *J Polym Sci B*. 1993;31(3):371-381.

SUPPORTING INFORMATION

Additional supporting information can be found online in the Supporting Information section at the end of this article.